JOURNAL OF THERMOPHYSICS AND HEAT TRANSFER
Vol. 23, No. 4, October–December 2009

Computational Analysis of Fluid Flow and Heat Transfer in Wire-Sandwiched Microheat Pipes

R. L. Rag* and C. B. Sobhan†
National Institute of Technology, Calicut 673 601, India

DOI: 10.2514/1.44101

The microheat pipe is a promising option in the thermal management of high-heat flux electronic components and packages. A computational analysis of wire-sandwiched (wire-bonded) microheat pipes, a relatively new design in microheat pipes, is presented in this paper. A transient one-dimensional model has been used in the analysis, which incorporates the longitudinal variation in the flow cross-sectional areas within the heat-pipe channel, frictional effects, and phase change during the process. The governing equations have been solved using a fully implicit finite difference scheme to obtain the velocity, pressure, and temperature distributions. These results are used to calculate and characterize the effective thermal conductivity of the heat pipe. The predicted results for the wire-sandwiched design are compared with those for the triangular cross section microheat pipe channel and discussed extensively.

Nomenclature

A	=	area of cross section, m^2
C	=	specific heat, J/kg K
D_H	=	hydraulic diameter of the channel, m
E	=	total energy per unit volume, J/m^3
f	=	friction factor
h_{lv}	=	latent heat of vaporization, J/kg
h_o	=	heat transfer coefficient, W/m^2 K
k	=	thermal conductivity, W/m K
L	=	length of the heat pipe, m
P	=	perimeter, m
P_w	=	pitch of the wires (center-to-center distance of the wire), m
p	=	pressure, Pa
Q	=	heat, W
q	=	heat flow rate, W/m^2
R	=	universal gas constant, J/kg K
Re	=	Reynolds number
$R_{\min}$	=	minimum meniscus radius, m
R_w	=	radius of the wire, m
r	=	radius of the meniscus, m
T	=	temperature, K
t	=	time, s
u	=	axial velocity, m/s
v	=	velocity, m/s
x	=	axial coordinate
α	=	contact angle, deg
ΔT	=	temperature difference, $T - T_{\text{amb}}$, K
μ	=	dynamic viscosity, kg/m s
ρ	=	density, kg/m^3
σ	=	surface tension, N/m

Subscripts

a	=	adiabatic section
amb	=	ambient
c	=	condenser section
e	=	evaporator section
eff	=	effective
h	=	hydraulic
i	=	interface
l	=	liquid
li	=	liquid interface
lw	=	liquid wall
sat	=	saturation
v	=	vapor
vi	=	vapor interface
vw	=	vapor wall

Received 3 March 2009; revision received 12 June 2009; accepted for publication 30 June 2009.

*Ph.D. Scholar, Department of Mechanical Engineering.
†Professor, School of Nano Science and Technology; csobhan@nitc.ac.in

Introduction

THE heat pipe is a passive heat transport device of highly effective thermal conductance that depends on the phase change of a working fluid and capillary action in a wick structure for its operation [1]. The construction and operation of the microheat pipe is more or less similar to the conventional heat pipe, except that it does not require a wick, but uses the sharp corners of its passage for the capillary circulation of the working fluid [2,3]. The concept of using microheat pipes for heat dissipation from semiconductor devices was first introduced by Cotter [2]. In general, passages with polygonal cross sections, which can provide sufficient capillary pressure difference for the flow of the liquid phase adjacent to their corners, can function as microheat pipes. The cross sections studied extensively in the literature are trapezoidal, rectangular, and triangular. On top of the applications in electronics cooling, microheat pipes also find a large number of other applications in various fields. They can be used for heat dissipation from laser diodes and other small localized heat generating devices and from photovoltaic cells. They are suitable for heat dissipation in association with microfabrication processes. Microheat pipes can be effective options for localized cooling of aircraft structures. In the biomedical field, they are recommended for heat removal and heat spreading associated with the treatment of carcinoma and control of epileptic seizures. Microheat pipes of various designs also have a significant role in space radiator recovery systems [3]. The wire-sandwiched (wire-bonded) microheat pipe is a relatively new design in microheat pipes [4], which uses a simple method to produce the flow passages, as will be described later.

The first steady-state model of the microheat pipe was developed by Cotter [2]. Based on this, Babin et al. [5] developed a steady-state model for trapezoidal microheat pipes to predict the maximum heat transport capacity, with conventional techniques outlined by Chi [6]. Khrustalev and Faghri [7] presented a detailed mathematical model

of the heat and mass transfer processes in microheat pipes with rectangular cross section, which described the liquid distribution and thermal characteristics as a function of the liquid charge. The predicted results were compared with experimental data obtained by Wu and Peterson [8] and Wu et al. [9]. A one-dimensional steady-state model for the evaporator and adiabatic sections of a triangular microheat pipe was developed by Longtin et al. [10] assuming constant vapor temperature throughout the length of the heat pipe. This analysis incorporated the interfacial shear stress and body-force terms in the momentum equation.

A steady-state mathematical model for the maximum heat transport capability of a microheat pipe, and temperature gradients that contribute to the overall temperature drop as a function of the heat transfer, was developed by Peterson and Ma [11]. The importance of this model was that it considered the governing equations for fluid flow and heat transfer in the evaporating thin-film region. The maximum heat transfer capacity of copper-water microheat pipes was explored by Hopkins et al. [12] using a one-dimensional model for predicting the capillary limitation. In this analysis, the liquid–vapor meniscus was divided into two regions depending on whether the contact angle is constant at the evaporator or varying along the adiabatic and condenser sections.

The first transient investigation of the microheat pipe was performed by Wu and Peterson [8]. Calculations indicated a major liquid flow reversal due to an imbalance of pressure, during the transient period. A mathematical model was developed by Ma et al. [13] for liquid friction factor for flow occurring in irregular grooves, relevant to microheat pipe geometry. This model considered interfacial shear stress due to the liquid–vapor frictional interaction. A transient model for a triangular microheat pipe consisting of an evaporator section and a condenser section was developed by Sobhan et al. [14]. The momentum and energy equations were solved, along with mass conservation equations, the Laplace–Young equation, and the state equations for the two phases. Sobhan and Peterson [15] further explored this model, solving the governing equations using an implicit method to avoid computational instabilities and to better analyze the performance of the heat pipe for a much wider range of parametric variations. A comprehensive review of the analysis of microheat pipes found in the literature and a quantitative comparison of the performance of various designs are presented in a recent publication [16].

The wire-sandwiched (wire-bonded) microheat pipe [3] is one of the latest innovations in microheat pipes, which is aimed at use in conventional electronic cooling applications and also in advanced applications such as in spacecraft. This device can be fabricated by sintering an array of wires between two thin metal sheets. The sharp corners formed between the plate and the wires serve as liquid arteries [3,4]. A few publications dealing with the theoretical analysis of the flow and heat transfer process in wire-sandwiched microheat pipes can be found in the literature [4,17]. Launay et al. [17] investigated the effects of contact angle, fluid type, corner angle, and fill charge on the performance of the wire-plate microheat pipe array, which were earlier conceptualized, modeled, and analyzed by Wang and Peterson [4] as wire-bonded microheat pipes to obtain the effects of various parameters on maximum heat transport capacity. However, these investigations did not incorporate the fluid cross-sectional area variation along the heat pipe as a function of the position, in the differential formulation. In the present study, an extensive numerical model is used to analyze the flow and heat transfer in the wire-sandwiched microheat pipe channel, considering the effects of the geometrical nature of the flow passages, by using governing equations derived for a variable area domain. The distributions of the field variables and the performance of the heat pipe are evaluated, and comparisons provided with triangular microheat pipe channels. The effects of various design and geometrical parameters on the performance are also studied. A comparison of the performance of the wire-sandwiched microheat pipe with and without an adiabatic section is also presented. In the analysis, a transient formulation is used to obtain the steady-state results through an implicit finite difference scheme. The results are presented and discussed in detail in the sections to follow.

Formulation

The construction of the wire-sandwiched microheat pipe, which is fabricated by sintering a wire array between two flat plates, is shown in Fig. 1. A schematic view of a wire-sandwiched microheat pipe [3] consisting of an array of channels, in which each channel serves as an individual heat transporting device, is shown in Fig. 1a. Figure 1b shows the sectional details of the device. The variations in the liquid and vapor area cross sections along the length are schematically shown at the beginning of the evaporator and the end of the condenser in Fig. 1c. A qualitative picture of the flow cross sections at the evaporator and condenser ends is also shown in Fig. 1, signifying the variation of areas of cross section of the flow streams along the heat pipe channel. The geometry of an individual wire-sandwiched microheat pipe channel is shown in Fig. 2. The microheat pipe can have an externally heated evaporator section, an adiabatic section with no external heat transfer, and a condenser section subjected to convective cooling. In the present analysis a one-dimensional model is used, as the major variation of the field variables (velocity, pressure, and temperature) in the fluids are in the longitudinal direction. It is also assumed that the thermophysical properties of the working fluid in both the liquid phase and the vapor phase are constant.

The mathematical formulation is based on the following assumptions:

1) Laminar flow prevails in both the vapor and the liquid in the microheat pipe.

2) A no-slip boundary condition exists in both the liquid and the vapor domains. To check whether continuum modeling with no slip is sufficient to analyze the problem, guidelines from the literature [18] have been used, and a calculation of the Knudsen number is performed. The molecular mean free path of water vapor is calculated as 3.034×10^{-6} m [18]. The Knudsen number given by the ratio of the mean free path of water vapor to the minimum dimension of the vapor core [18] (this is the diameter of vapor core at the condenser end, which corresponds to the diameter of a circle equal to the wire diameter, as shown in Fig. 1c) is calculated as 3.7925×10^{-3}. Because the value of the Knudsen number is less than 0.01, continuum formulation with no-slip boundary condition was used, as suggested in the literature [18].

3) The vapor is at its saturation pressure, corresponding to the working temperature.

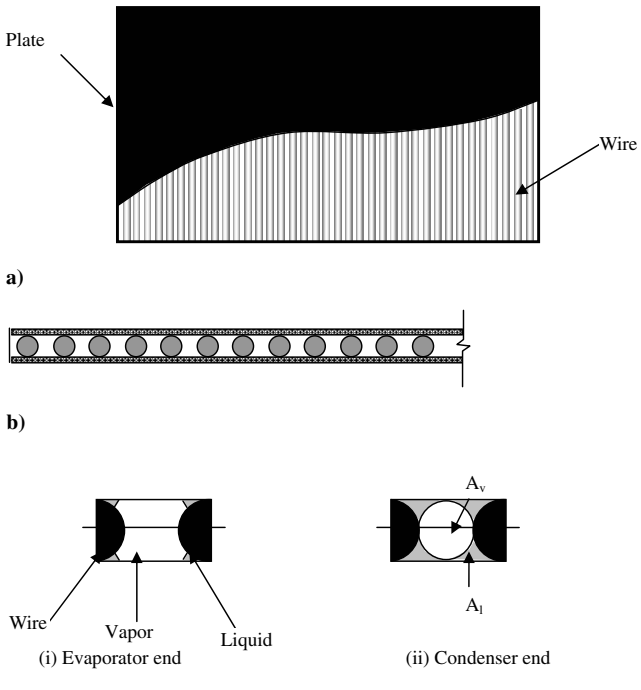

Fig. 1 Schematic of the wire-sandwiched microheat pipe construction [3,4].

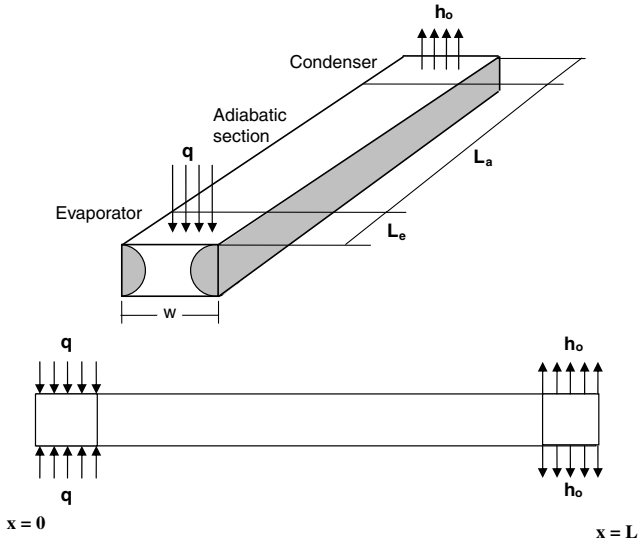

Fig. 2 Configuration of a single microheat pipe in the array.

The governing equations include the Laplace–Young equation containing the local meniscus radius of the vapor-liquid interface, in addition to the differential equations for mass, momentum, and energy conservation. The interfacial mass balance equation is also built-in into the governing differential equations. The equation of state, with an ideal gas assumption, is used to link between the pressure and temperature of the vapor [14]. For the liquid, the first approximation used for the pressure computation is the Hagen–Poiseuille equation, which is subsequently corrected iteratively by substituting in the momentum equation. The methodology of the mathematical formulation is similar to that used for the analysis of a triangular microheat pipe, as presented in [14], but the geometry of the passages is different in the present case. The governing differential equations are derived for a varying area domain.

The mathematical formulation for flow and heat transfer in the passages formed by the wire-sandwiched geometry is presented in the next section. The general governing equations have been presented earlier in the literature while analyzing triangular microheat pipes [14] and are reproduced here. It is to be noted that in the present case, the geometry of the passages is different. The method to calculate the fluid cross-sectional areas for the relevant geometry of the passages in between the wires, as a function of the longitudinal distance, is also explained in the next section.

The mass, momentum, and energy conservation equations are used in the mathematical model. The continuity equation for both the vapor and liquid phases for the evaporator, adiabatic, and the condenser sections are shown in Table 1. The vapor and liquid momentum equations are shown in Table 2. The energy equations for both the liquid and vapor phases for all the sections of the microheat pipe are given in Table 3. Schematic diagrams of the control volumes pertinent to the equations are also shown in the tables. Other than the conservation equations, the following equations are also used in the formulation of the problem:

Laplace–Young equation,

$$p_v - p_l = \frac{\sigma}{r} \tag{1}$$

Equation of state for the vapor,

$$p_v = \rho_v R_v T_v \tag{2}$$

Hagen–Poiseuille equation as first approximation for the liquid flow,

$$(\partial p_l/\partial x) = [8\mu_l u_l/(D_H^2/4)] \tag{3}$$

Boundary conditions at $x = 0$ and $x = L$,

$$u_l = 0; \qquad u_v = 0; \qquad \frac{\partial T}{\partial x} = 0 \tag{4}$$

At $x = 0$,

$$p_v - p_l = \frac{\sigma}{r_{\min}} \tag{5}$$

The minimum meniscus radius is taken from literature as 32×10^{-5} m [4].

Initial conditions:

At $t = 0$, for all x,

$$p_v = p_l = p_{\text{sat}}; \qquad T_v = T_l = T_{\text{sat}} \tag{6}$$

The friction factors in the governing equations can be generally expressed as

$$f = \frac{k}{Re} \tag{7}$$

where k is a constant that depends on the geometry of heat pipe channel.

Table 1 Mass conservation equations

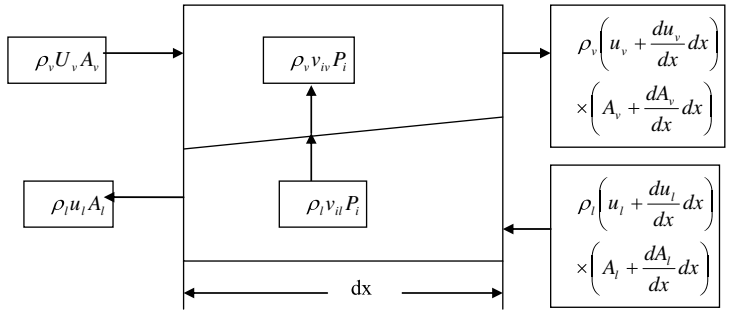

CV for mass conservation

Vapor continuity equation

For evaporator section	For adiabatic section	For condenser section
$A_v \frac{du_v}{dx} + u_v \frac{dA_v}{dx} + P_i v_{iv} = 0$	$A_v \frac{du_v}{dx} + u_v \frac{dA_v}{dx} = 0$	$A_v \frac{du_v}{dx} + u_v \frac{dA_v}{dx} - P_i v_{iv} = 0$

Liquid continuity equation

For evaporator section	For adiabatic section	For condenser section
$A_l \frac{du_l}{dx} + u_l \frac{dA_l}{dx} - P_i v_{il} = 0$	$A_l \frac{du_l}{dx} + u_l \frac{dA_l}{dx} = 0$	$A_l \frac{du_l}{dx} + u_l \frac{dA_l}{dx} + P_i v_{il} = 0$

Table 2 Momentum conservation equations

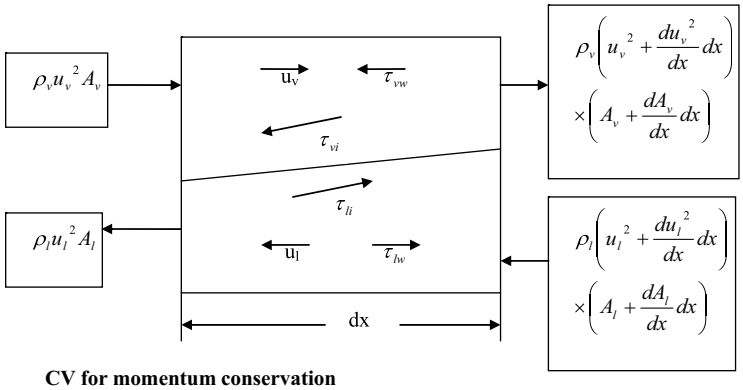

CV for momentum conservation

Vapor momentum equation

$$\rho_v[u_v^2\tfrac{\partial A_v}{\partial x}+2A_v u_v\tfrac{\partial u_v}{\partial x}]+A_v\tfrac{\partial p_v}{\partial x}+\rho_v A_v g\sin\theta-\tfrac{1}{2}P_{vw}\rho_v u_v^2 f_{vw}-\tfrac{1}{2}P_i\rho_u u_v^2 f_{iv}=\rho_v A_v\tfrac{\partial u_v}{\partial t}$$

Liquid momentum equation

$$-\rho_l[u_l^2\tfrac{\partial A_l}{\partial x}+2A_l u_l\tfrac{\partial u_l}{\partial x}]-A_l\tfrac{\partial p_l}{\partial x}+\rho_l A_l g\sin\theta-\tfrac{1}{2}P_{lw}\rho_l u_l^2 f_{lw}-\tfrac{1}{2}P_i\rho_l u_l^2 f_{il}=\rho_l A_l\tfrac{\partial u_l}{\partial t}$$

The cross section of the vapor passage varies continuously in the evaporator and the condenser sections. The vapor cross section can be assumed almost rectangular in the evaporator and circular in the condenser section, as shown in Fig. 1c. The value of k for vapor core is taken as an average of that for the rectangular and the circular sections. The liquid is assumed to flow through an almost triangular cross section adjacent to the corners. Therefore, k for the liquid is taken as that for a triangular cross section passage. The appropriate values for k corresponding to the geometries mentioned previously are obtained from the literature [19].

The geometric configuration of the vapor and liquid flow passages produce an interface meniscus as represented in Fig. 3. The areas of the liquid and the vapor cross sections, which vary continuously along the length due to progressive phase change as the fluid flows along the channel, are expressed in terms of interfacial meniscus radius as derived geometrically in Fig. 3.

Area of liquid

$$A_l=8R_w r_m\mathrm{Sin}\beta_1\mathrm{Sin}\beta_2-4R_w^2(\beta_1-\mathrm{Sin}\beta_1\mathrm{Cos}\beta_1)-4r_m^2(\beta_2-\mathrm{Sin}\beta_2\mathrm{Cos}\beta_2) \tag{8}$$

Area of vapor

$$A_v=R_w(2w-\pi R_w)-A_l \tag{9}$$

Liquid–vapor interface perimeter

$$p_{iv}=p_{il}=8r_m\beta_2 \tag{10}$$

Table 3 Energy conservation equations

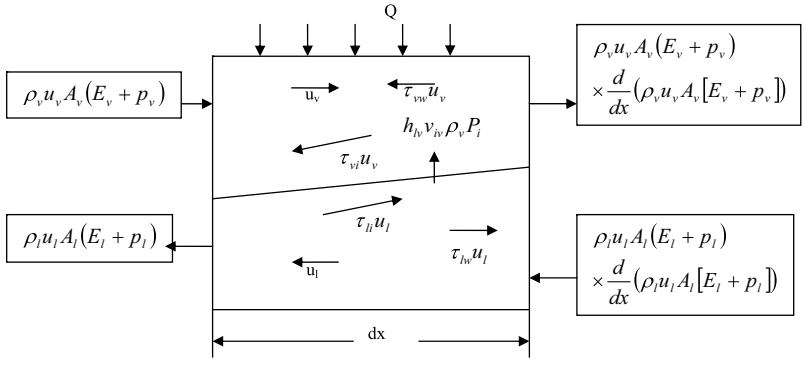

CV for energy conservation

Vapor Energy equations

For Evaporator Section

$$A_v\tfrac{\partial E_v}{\partial t}+\tfrac{\partial}{\partial x}[u_v A_v(E_v+p_v)]=\tfrac{\partial}{\partial x}\{\tfrac{4}{3}\mu_v u_v A_v\tfrac{\partial u_v}{\partial x}+K_v A_v\tfrac{\partial T_v}{\partial x}\}+qP_{vw}+h_{lv}v_{iv}\rho_v P_i+\tfrac{1}{2}\rho_v u_v^2 f_{iv}u_v p_{iv}+\tfrac{1}{2}\rho_v u_v^2 f_{vw}u_v P_{vw}\ \text{Where}\ E_v=\rho_v(c_v T+\tfrac{1}{2}u_v^2)$$

For Adiabatic Section

$$A_v\tfrac{\partial E_v}{\partial x}+\tfrac{\partial}{\partial x}[u_v A_v(E_v+P_v)]=\tfrac{\partial}{\partial x}\{\tfrac{4}{3}\mu_v u_v A_v\tfrac{\partial u_v}{\partial x}+K_v A_v\tfrac{\partial T_v}{\partial x}\}+\tfrac{1}{2}\rho_v u_v^2 f_{iv}u_v p_{iv}+\tfrac{1}{2}\rho_v u_v^2 f_{vw}u_v P_{vw}$$

For Condenser Section

$$A_v\tfrac{\partial E_v}{\partial t}+\tfrac{\partial}{\partial x}[u_v A_v(E_v+p_v)]=\tfrac{\partial}{\partial x}\{\tfrac{4}{3}\mu_v u_v A_v\tfrac{\partial u_v}{\partial x}+K_v A_v\tfrac{\partial T_v}{\partial x}\}+h_0 P_{vw}\Delta T-h_{lv}v_{iv}\rho_v P_i+\tfrac{1}{2}\rho_v u_v^2 f_{iv}u_v P_{iv}+\tfrac{1}{2}\rho_v u_v^2 f_{vw}u_v P_{vw}$$

Liquid Energy Equations

For Evaporator Section

$$A_v\tfrac{\partial E_l}{\partial t}+\tfrac{\partial}{\partial x}[u_l A_l(E_l+p_l)]=\tfrac{\partial}{\partial x}\{\tfrac{4}{3}\mu_l u_l A_l\tfrac{\partial u_l}{\partial x}+K_l A_l\tfrac{\partial T_l}{\partial x}\}+qP_{lw}+h_{lv}v_{iv}\rho_l P_i+\tfrac{1}{2}\rho_l u_l^2 f_{il}u_l P_i+\tfrac{1}{2}\rho_l u_l^2 f_{lw}u_l P_{lw}$$

For Adiabatic Section

$$A_l\tfrac{\partial E_l}{\partial t}+\tfrac{\partial}{\partial x}[u_l A_l(E_l+p_l)]=\tfrac{\partial}{\partial x}\{\tfrac{4}{3}\mu_l u_l A_l\tfrac{\partial u_l}{\partial x}+K_l A_l\tfrac{\partial T_l}{\partial x}\}+\tfrac{1}{2}\rho_l u_l^2 f_{il}u_l p_{iv}+\tfrac{1}{2}\rho_l u_l^2 f_{il}u_l P_{lw}$$

For Condenser Section

$$A_v\tfrac{\partial E_l}{\partial t}+\tfrac{\partial}{\partial x}[u_l A_l(E_l+p_l)]=\tfrac{\partial}{\partial x}\{\tfrac{4}{3}\mu_l u_l A_l\tfrac{\partial u_l}{\partial x}+K_l A_l\tfrac{\partial T_l}{\partial x}\}-h_0 P_{lw}\Delta T+h_{lv}v_{iv}\rho_l P_i+\tfrac{1}{2}\rho_l u_l^2 f_{il}u_l P_i+\tfrac{1}{2}\rho_l u_l^2 f_{lw}u_l P_{lw}$$

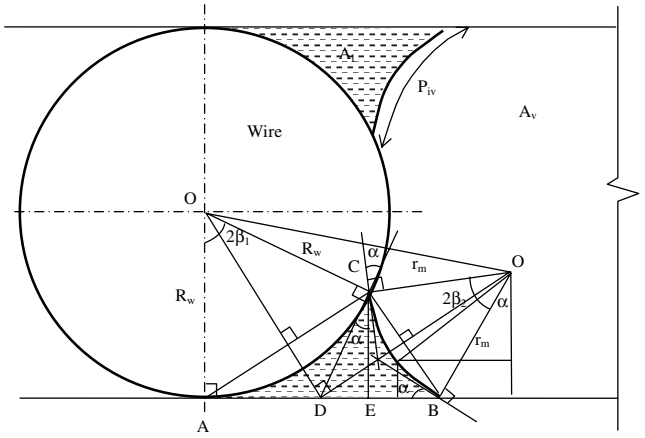

Fig. 3 Geometry of the interface meniscus in the wire-sandwiched microheat pipe [22].

Liquid-wall contact area

$$p_l = 2R_w(\beta_1 + \tan\beta_1) \tag{11}$$

Vapor-wall contact area

$$p_v = 2(w + \pi R_w) + 8(r_m\beta_2 - R_w\tan\beta_1 - R_w\beta_1) \tag{12}$$

Relation between α, β_1, and β_2

$$\beta_1 + \beta_2 + \alpha = \frac{\pi}{2} \tag{13}$$

$$R_w\mathrm{Sin}^2\beta_1 = r_m\mathrm{Cos}\beta_1\mathrm{Sin}\beta_2 \tag{14}$$

$$\beta_1 = \tan^{-1}\left(\left(\frac{1}{2R_w}\right)\{-r_m\mathrm{Sin}\alpha + [(r_m\mathrm{Sin}\alpha)^2 + 4R_w r_m\mathrm{Cos}\alpha]^{\frac{1}{2}}\}\right) \tag{15}$$

The constructional details of the microheat pipe considered in the analysis and the properties of the working fluid are given in Table 4.

Solution Procedure

The governing equations were solved using a fully implicit finite difference scheme, based on central differences, using a code developed in-house. The steps involved in the solution procedure of the numerical scheme have been discussed in the literature [13] while analyzing a triangular microheat pipe, and are summarized in the following list.

1) Obtain the local meniscus radius using the Laplace–Young equation.

2) Using the vapor momentum equation, obtain the axial vapor velocity.

3) Obtain the interfacial vapor velocity using the vapor continuity equation and calculate the interfacial liquid velocity applying the interface mass balance.

4) Obtain the vapor temperature from the vapor energy equation.

5) Calculate the vapor pressure using the equation of state for the vapor.

6) From the liquid continuity equation, obtain the liquid velocity derivatives in terms of the interfacial liquid velocity and substitute them in the liquid momentum equation. Solve the liquid momentum equation to obtain the axial liquid velocity.

7) Calculate the liquid pressure using the Hagen–Poiseuille equation. Substitute the liquid pressure again in the liquid momentum equation and iterate for spatial convergence.

8) Obtain the liquid temperature from the liquid energy equation.

9) Continue time stepping to obtain steady-state results.

The computation was performed using successive underrelaxation in all the field variables to suppress divergence. Stable and converged results were obtained through successive refinement of space and time steps.

Table 4 Details of the physical problem

Solid material	Copper
Working fluid	Water
Length of the heat pipe	125 (baseline case), 120, 121, 122, 123, 124, 127.5, 128, 130 mm
Radius of wire	0.8 (baseline case), 0.825, 0.85, 0.875, 0.9 mm
Pitch of the wires	2.0 (baseline case), 2.1, 2.2, 2.3, 2.4 mm
Length of the evaporator	20 mm
Length of the adiabatic section	85 (baseline case), 82–88 mm
Length of the condenser	20 (baseline case), 15, 16, 17, 18, 19, 20, 22.5, 25 mm
Density of vapor	0.0256 kg/m^3 [20]
Density of liquid	998.2 kg/m^3 [20]
Thermal conductivity of liquid	0.613 W/m K [20]
Thermal conductivity of vapor	19.6×10^{-3} W/m K [20]
Viscosity of liquid	1.003×10^{-3} N s/m^2 [20]
Viscosity of vapor	9.09×10^{-6} N s/m^2 [20]
Surface tension	0.0718 N/m [20]

Results and Discussion

To benchmark the formulation and computation procedure, the calculated maximum evaporator temperature ($Te_{,max}$), average temperature of the adiabatic section ($Ta_{,ave}$), and the minimum condenser temperature ($Tc_{,min}$) at the steady state have been compared with the corresponding experimental results available in the literature for a wire-sandwiched microheat pipe [4], for different input heat flux values in the range 0.4133 to 0.41330 − .62 W/cm^2 and a wire diameter of 0.813 mm. As reported in the experimental study in the literature [4], the condenser end was kept at a temperature of 313 K in the calculation also. As the material-fluid combination used in the experimental study was different (acetone-aluminum system), a qualitative comparison could be made between the two cases. In spite of these differences the results are found to match fairly well, and show similar trends as depicted in Fig. 4. The calculated temperature values were also compared with reported experimental results on wire-sandwiched heat pipes, as shown in Fig. 5, where the experiments were aimed at obtaining the dryout length [16], though the heating levels in this work were higher than those in the present case. Here, though the dimensional and operational parameters are different, the nature and trends of the temperature distribution agree well qualitatively with the experimental results.

The computational accuracy is checked by conducting a grid-independence study using a different number of special steps between 250 and 350 in the domain of analysis. Figure 6 shows the attainment of grid independence, where successive refinement of the grids does not produce significant difference in the computed values, which indicates stable and converged results. The maximum difference between the computed values of temperature can be seen to be less than 0.5% between 325 and 350 nodal points in the domain; therefore, 350 nodes were taken in the computation.

Along with the convergence in the field variables, the overall energy balance at the steady state was also verified to check the accuracy of the model, by checking the equality of the heat input at the evaporator and dissipation at the condenser. Figure 7 shows the transient variation of heat dissipation at the condenser section, in which the balance with the input heat serves as an indication of attainment of steady state and the overall accuracy of computation.

Distributions of the Field Variables

The radius of curvature of the liquid–vapor meniscus plays an important role in determining the heat pipe performance. The fluid area parameters that have direct impact on the field variables are dependent on the meniscus radius along the heat pipe. The Laplace–

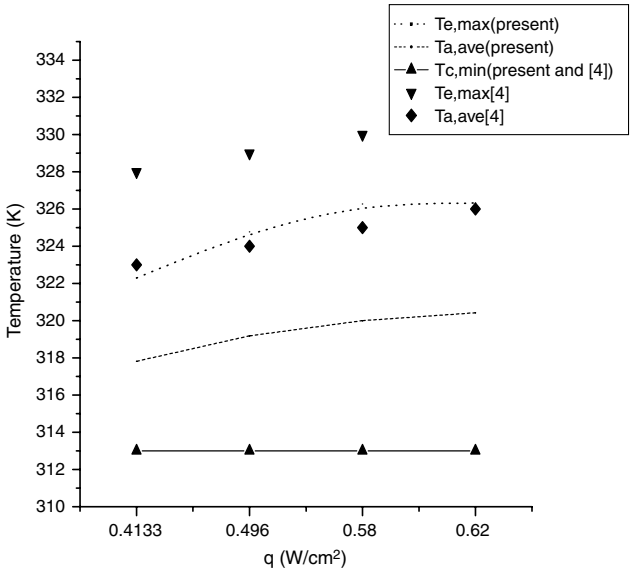

Fig. 4 Comparison of maximum evaporator temperature $Te_{,max}$, average temperature of the adiabatic section ($Ta_{,ave}$), and minimum condenser temperature ($Tc_{,min}$) of the present model for different input heat flux values, with experimental values in literature [4].

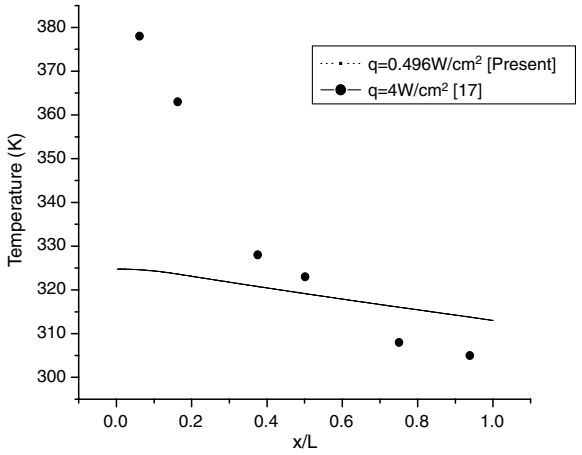

Fig. 5 Comparison of the temperature profile with that available in literature [17] with higher heating levels.

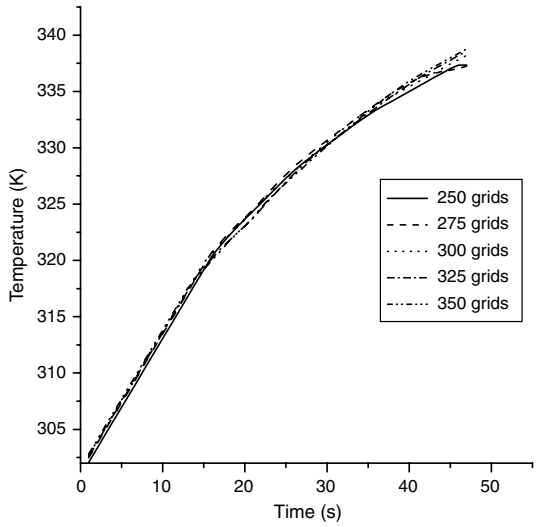

Fig. 6 Transient variation of temperature for different grid sizes for an input heat flux of 2.5 W/cm² and a condenser heat transfer coefficient of 550 W/m² K.

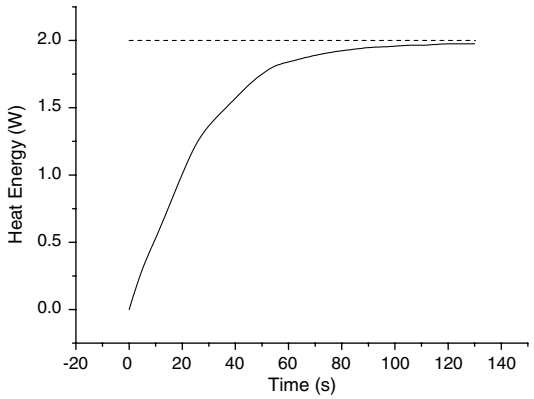

Fig. 7 Transient variation of heat transfer at the condenser section for an input heat flux of 2.5 W/cm² and a condenser heat transfer coefficient of 550 W/m² K. The calculated heat input at the evaporator section corresponding to the baseline case is 2 W. The energy balance at the steady state is obvious.

Young equation was solved along with the other governing equations by incorporating the computed pressures, proceeding to the steady state to obtain the meniscus radius at each step. The typical steady-state meniscus radius distribution is shown in Fig. 8. As the pressure difference between the vapor and the liquid becomes progressively smaller from the evaporator to the condenser as will be shown later, there is a corresponding increase in the meniscus radius. The nature of variation of the meniscus radius is found to agree with that for a triangular microheat pipe with only the evaporator and the condenser sections, analyzed in the literature [14]. In the present case, the absence of phase change and heat transfer at the adiabatic section creates a linear variation for the meniscus radius whereas at the evaporator and the condenser sections, the variations are as shown in Fig. 8.

The distributions of the liquid and vapor velocities in the wire-sandwiched microheat pipe with and without an adiabatic section are shown in Figs. 9a–9d. The vapor velocity increases in the evaporator section due to the mass addition and decreases in the condenser section because of depletion of mass, as expected. Similarly, as liquid flows from the condenser to the evaporator, liquid velocity increases along the condenser section and decreases in the evaporator section. The values of the velocity of the liquid are lower than those of the vapor due to the appreciable difference in densities between the two media. The liquid velocity values are negative, indicating the direction of flow of the liquid. The vapor and liquid velocity distributions for a wire-sandwiched microheat pipe that consists of an adiabatic section are similar in both the evaporator and the condenser regions with comparatively smaller velocity gradients at the adiabatic sections, as no major mass addition or depletion takes place in the

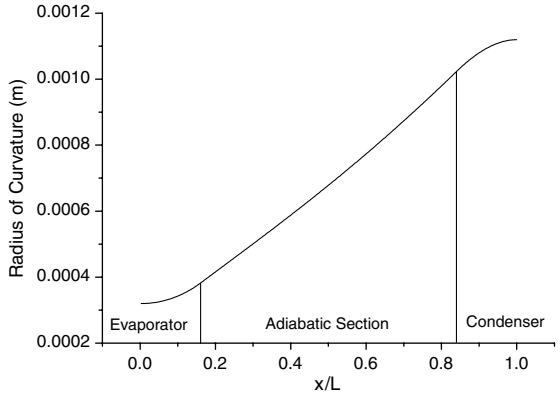

Fig. 8 Distribution of the radius of curvature of the liquid–vapor interface meniscus along the microheat pipe. The graph corresponds to an input heat flux of 2.5 W/cm² and a condenser heat transfer coefficient of 550 W/m² K.

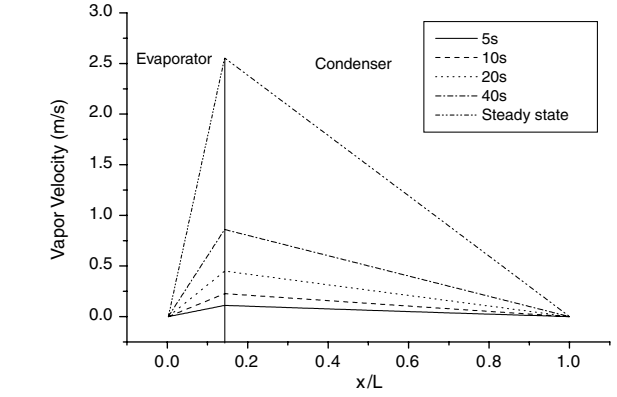

a)

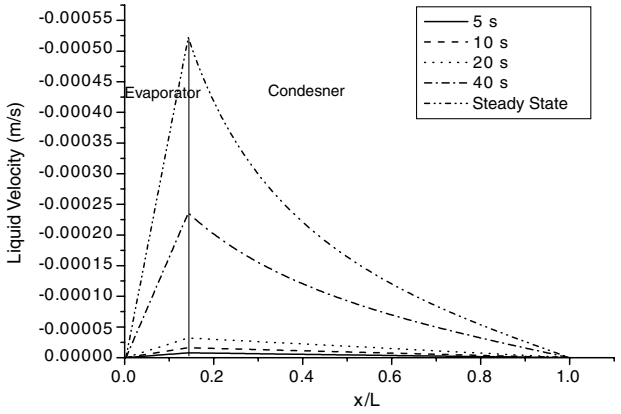

b)

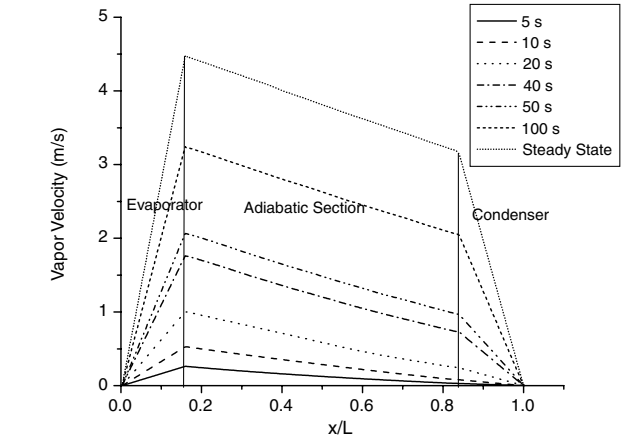

c)

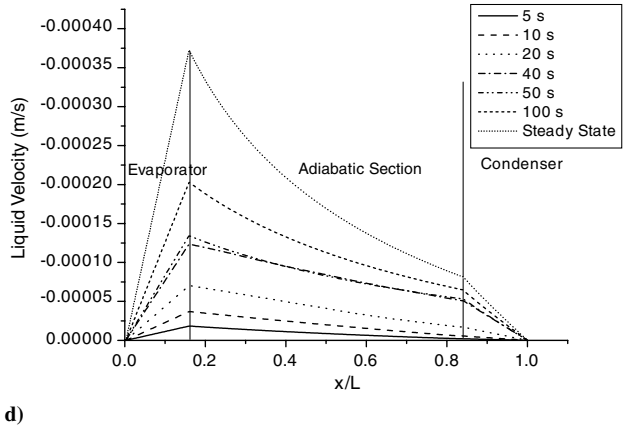

d)

Fig. 9 Velocity distributions in the wire-sandwiched microheat pipe. The heat input is 2.5 W/cm^2 and the condenser heat transfer coefficient is 550 W/m^2 K.

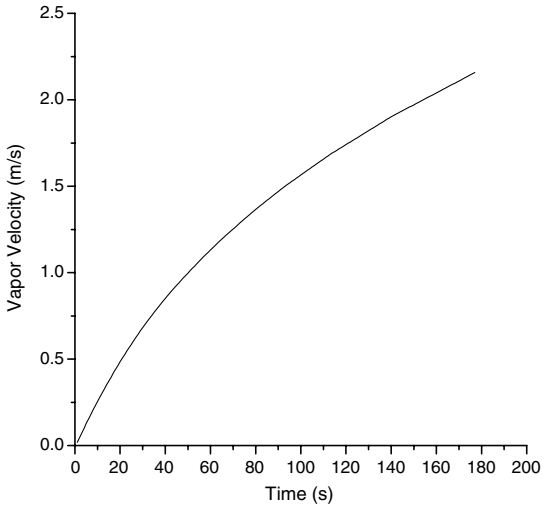

Fig. 10 Transient variation of the vapor velocity in a wire-sandwiched microheat pipe with an input heat flux of 2.5 W/cm^2 and a condenser heat transfer coefficient of 550 W/m^2 K.

adiabatic section due to the absence of external heating or cooling. The transient velocity variation is shown in Fig. 10, which clearly indicates that the velocity values grow with respect to time, until reaching the steady state.

Figures 9c and 9d further indicate that the physical effects at the evaporator and the condenser sections have an influence on the adiabatic section also. This produces a velocity variation in the adiabatic section, which is the outcome of the small amount of phase change happening in this section. The penetration of the effect of the evaporator and the condenser into the adiabatic section in a heat pipe has been identified and discussed extensively earlier, in relation to the variation in velocity and temperature in the adiabatic section of flat heat pipes [21].

The steady-state vapor and liquid pressure distributions in the microheat pipe are shown in Fig. 11. The pressure drop in the liquid portion is found to be larger than that in the vapor, owing to the large density of the liquid compared with that of the vapor. The variations as shown are typical of microheat pipes, and have been observed in microheat pipes of triangular cross section also [14,15].

The vapor temperature distribution obtained is similar to the pressure distribution, as the equation of state for the ideal gas is used. As discussed earlier, the effect of the evaporator section in the temperature propagates into the adiabatic section also. Because of this, the temperature drop at the junction between the evaporator and adiabatic section is not abrupt. Similarly the effect of the condenser also propagates into the adiabatic section. Figure 12a shows the transient growth of the temperature distribution along the heat pipe. As expected, the temperature drop for a given input heat flux becomes smaller as time proceeds, indicating a transient increase in

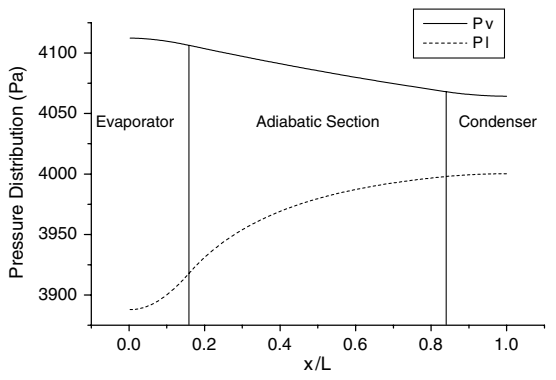

Fig. 11 Longitudinal pressure distribution in the wire-sandwiched microheat pipe. The heat input is 2.5 W/cm^2 and the condenser heat transfer coefficient is 550 W/m^2 K.

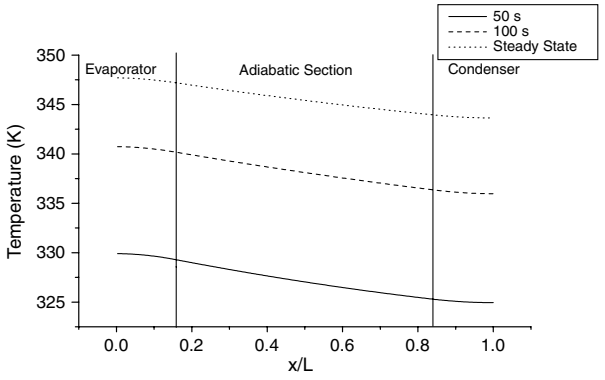

a)

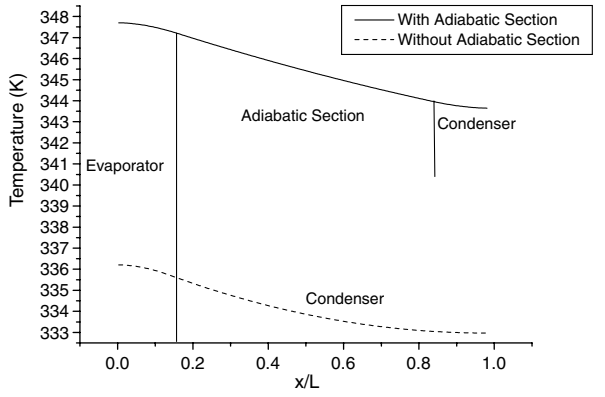

b)

Fig. 12 Temperature distribution in the wire-sandwiched microheat pipe with an input heat flux of 2.5 W/cm^2 and a condenser heat transfer coefficient of 550 W/m^2 K.

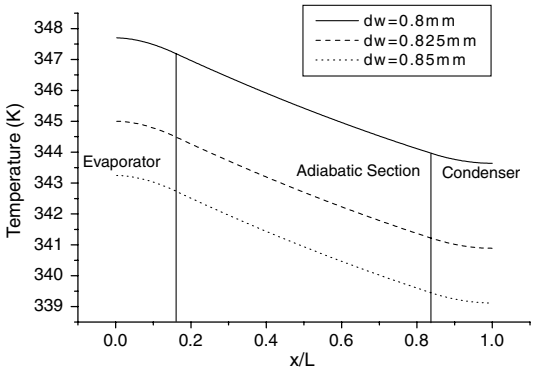

a)

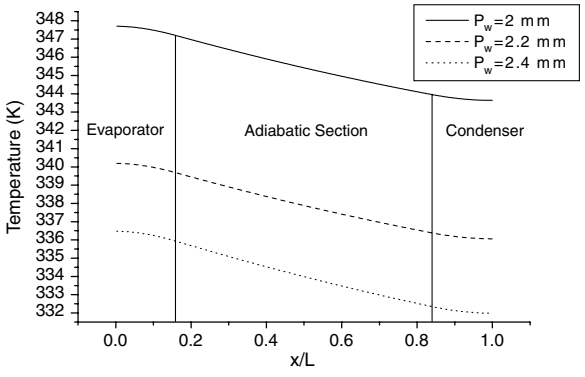

b)

Fig. 13 Effect of the channel geometry on the steady-state temperature distribution in the wire-sandwiched microheat pipe for an input heat flux of 2.5 W/cm^2 and a condenser heat transfer coefficient of 550 W/m^2 K.

the effective thermal conductivity. This effect has also been observed in the case of triangular microheat pipe [14,15]. Figure 12b compares the temperature distributions in wire-sandwiched microheat pipes with and without an adiabatic section. Because of the absence of phase change, the temperature distribution has an almost linear variation in the adiabatic section. In the case of a wire-sandwiched microheat pipe without an adiabatic section, an exactly similar nature of temperature variation is seen, as in the triangular microheat pipe without an adiabatic section reported in the literature [14,15].

Effect of Geometrical Parameters on Steady-State Temperature Distribution

The geometrical parameters considered in the present study are the wire diameter, the pitch of the wires (center-to-center distance), the length of the adiabatic section, and the length of condenser section. The length of the evaporator section is kept constant, and this represents the dissipating surface area of a heat source to which the heat pipe heat sink is attached. The influence of the wire diameter on the temperature distributions is shown in Fig. 13a. The temperature drop increases slightly as the wire diameter is increased. Figure 13b shows a similar nature of variation for an increase in the pitch of the wires. In both these cases, the increase in the geometrical parameters dimensions enhances the flow cross-sectional area, which in turn reduces the vapor velocity. This decrease in velocity reduces the phase change and the heat transport, the effect of which is understood to be one of the reasons for the increase of the temperature drop between the ends of the microheat pipe. Another reason could be the reduction of viscous forces and associated energy dissipation while the flow cross-sectional area is reduced, which produces a slightly larger temperature drop between the ends of the heat pipe. However, though the temperature drops are slightly increased, the evaporator temperature is reduced considerably due to an increase in these parameters. This is a desirable effect in electronics cooling applications.

The temperature distributions in wire-sandwiched microheat pipes with different lengths for the adiabatic section are shown in Fig. 14. For identical evaporator and condenser lengths, an increase in the length of the adiabatic section produces a decrease in the temperature drop between the evaporator and condenser ends, which produces a flatter temperature distribution. At the same time, the temperature level is considerably increased due to an increase in the length of the adiabatic section. An increase in the length of the condenser, on the other hand, enhances the temperature drop between the extreme ends, as shown in Fig. 15. In both the cases there are corresponding variations in the effective lengths of the microheat pipe.

Performance Evaluation

The effective thermal conductivity is a performance indicator that helps to compare heat pipes or microheat pipes with various designs

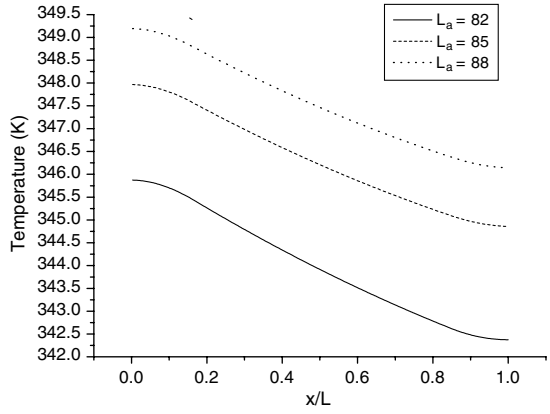

Fig. 14 Steady-state temperature distributions for different lengths of the adiabatic section, for an input heat flux of 2.5 W/cm^2 K and a condenser heat transfer coefficient of 550 W/m^2 K.

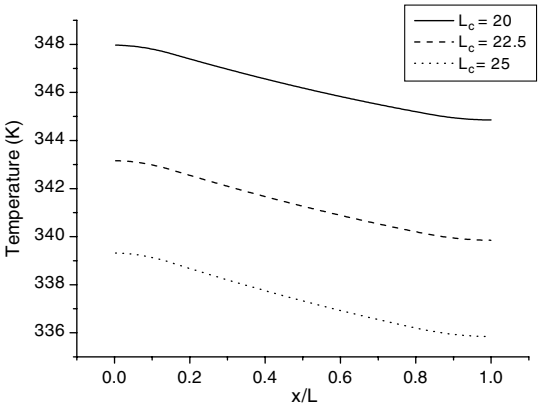

Fig. 15 Steady-state temperature distributions for different lengths of the condenser section, for an input heat flux of 2.5 W/cm^2 K and a condenser heat transfer coefficient of 550 W/m^2 K.

at different operating conditions. The effective thermal conductivity is defined on the basis of the Fourier law of heat conduction as follows [14,15]:

$$k_{\text{eff}} = \frac{q_{in}}{A_c \frac{\Delta T}{L}} \tag{16}$$

From the temperature distribution, the effective conductivity has been calculated for the wire-sandwiched microheat pipe. The effects of various operational and geometrical parameters on the effective thermal conductivity, through the calculated points and trend lines, are shown in Figs. 16–19. Figure 16 shows the variation of the effective thermal conductivity with respect to the heat input to the evaporator. As the heat input is increased, the effective conductivity

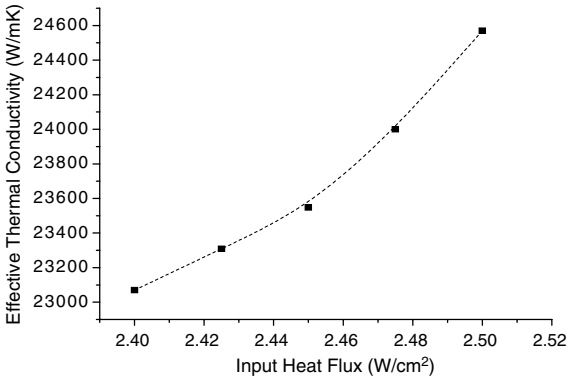

Fig. 16 Variation of the effective thermal conductivity with the input heat flux, for a condenser heat transfer coefficient of 550 W/m^2 K.

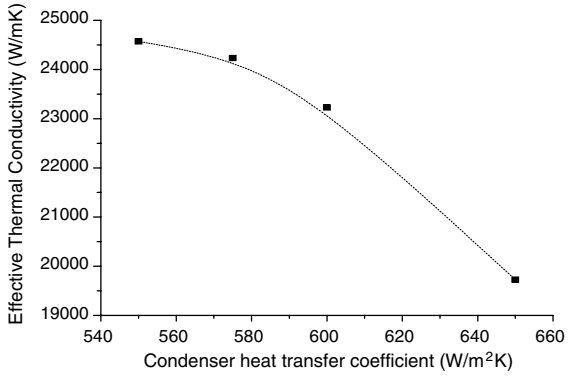

Fig. 17 Variation of the effective thermal conductivity with the condenser heat transfer coefficient, for an input heat flux of 2.5 W/cm^2.

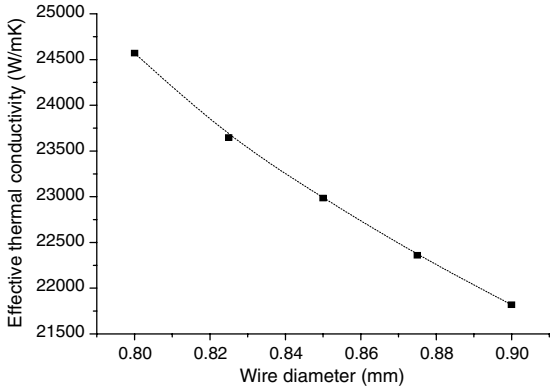

Fig. 18 Variation of effective thermal conductivity with the wire diameter, for an input heat flux of 2.5 W/cm^2 and a condenser heat transfer coefficient of 550 W/m^2 K.

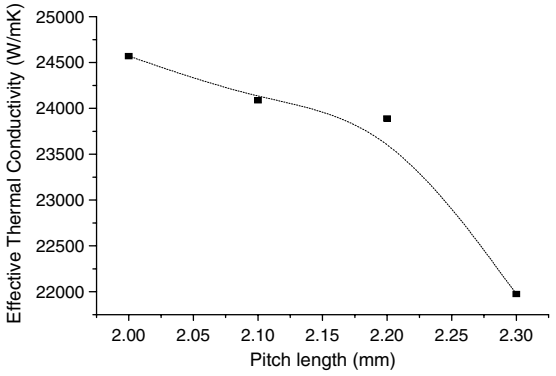

Fig. 19 Variation of the effective thermal conductivity with the pitch of the wires, for an input heat flux of 2.5 W/cm^2 and a condenser heat transfer coefficient of 550 W/m^2 K.

is also found to increase, as expected. This reflects a reduction in the temperature drop along the heat pipe as the input heat is increased. As the heat input and the corresponding temperature of operation increase in the heat pipe, the phase change and flow effects inside the device become more and more prominent. As a result of this, the heat pipe operates closer to an isothermal device, which translates into an increase in the effective thermal conductivity. This effect has also been observed in conventional heat pipes and microheat pipes of other cross sections, and indicates that it would be most effective to operate the heat pipe as close to the highest possible value of the heat input, limited only by the operating limits of the heat pipe [3,14]. The cross-sectional area of the triangular heat pipe array referred to here is 2×10^{-5} m^2 and the hydraulic mean diameter is 8.62×10^{-6} m. The heat pipe had an equilateral triangular cross section with side 0.3 mm. There is a decrease in the effective thermal conductivity with an increase in the condenser heat transfer coefficient, as shown in Fig. 17. This is due to an increased temperature drop of the microheat pipe in the axial direction, as the condenser heat transfer coefficient is increased. Though this increased temperature drop does not affect the heat transport, this makes the heat pipe surface less isothermal and might not be a preferable condition where an isothermal surface is required, such as in micro electronic applications. The nature of variation observed is similar to that in the case of the triangular microheat pipe reported earlier in the literature [15]. An increase in the wire diameter and the pitch of the wires both show a reduction in the effective thermal conductivity. The increased temperature drop along the heat pipe, in both these cases, reduces the effective thermal conductivity as shown in Figs. 18 and 19.

When the wire diameter is increased, both the liquid and vapor areas of cross section increase. This is one of the reasons why the flow velocities are reduced and, correspondingly, the phase change and the related heat transfer are retarded. Further, the increase in

Table 5 Effect of change in the wire diameter and pitch on the flow areas and the effective thermal conductivity values

Geometric parameter	Dimension (mm)	Liquid cross-sectional area at the end of the condenser A_l, mm^2	Vapor cross-sectional area at the end of the condenser A_v, mm^2	Total cross-sectional area of the flow passage at the end of the condenser, mm^2	K_{eff}, W/m K
Wire diameter	0.8	0.2315	0.8658	1.0973	24,570
	0.825	0.2389	0.8765	1.1154	23,647
	0.85	0.2462	0.8863	1.1325	22,647
	0.875	0.2535	0.8952	1.1487	22,361
	0.9	0.2606	0.9032	1.1638	21,819
Pitch	2.0	0.2315	0.8658	1.0973	24,570
	2.1	0.2315	0.9458	1.1813	24,088
	2.2	0.2315	1.0268	1.2583	23,889
	2.3	0.2315	1.1058	1.3363	21,935

dimensions of the flow path reduces the viscous effects, which also may be partially responsible for the increase in the temperature drop between the ends and corresponding reduction of the effective thermal conductivity.

Because of the geometry of the flow passage as shown in Fig. 1, a change in the pitch of the wires does not affect the liquid cross section area as the corner shape is unaffected by this. This implies that a change in the wire pitch affects only the vapor flow area, and the effect on effective thermal conductivity is essentially a result of this. The effects of a change in the wire diameter and pitch of the wires on the cross-sectional areas of the liquid and the vapor at the condenser end are shown in Table 5. The corresponding values of the effective thermal conductivity are also shown in the table. The nature of the variation of the values as shown in Figs. 18 and 19 would be useful in the geometrical design of wire-sandwiched microheat pipes, and in predicting the performance of the device.

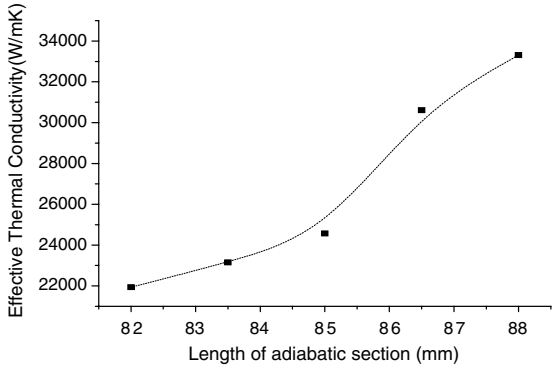

Fig. 20 Variation of effective thermal conductivity with variation in the length of adiabatic section, for an input heat flux of 2.5 W/cm^2 and a condenser heat transfer coefficient of 550 W/m^2 K for a wire diameter of 0.8 mm and pitch 2.0 mm.

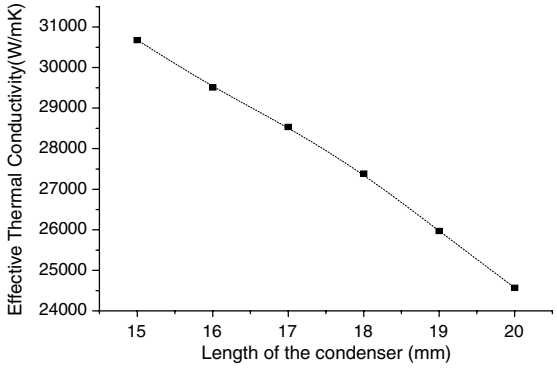

Fig. 21 Variation of effective thermal conductivity with variation in the condenser length, for an input heat flux of 2.5 W/cm^2 and a condenser heat transfer coefficient of 550 W/m^2 K for a wire diameter of 0.8 mm and pitch 2.0 mm.

Table 6 Comparison of performance of a wire-sandwiched microheat pipe and a triangular microheat pipe

	Effective thermal conductivity K_{eff}, W/m K	
Input heat flux, W/cm^2	Triangular microheat pipe array of cross-sectional area 2×10^{-5} mm^2 and length 140 mm [14]	Wire-sandwiched microheat pipe of cross-sectional area 2×10^{-5} mm^2 and length 140 mm [present study]
2.4	92,400	114,064
2.45	94,325	116,439
2.5	96,250	118,560

The influence of the length of the adiabatic section on the effective thermal conductivity is shown in Fig. 20. It is seen that an increase in the length of the adiabatic section produces an increase in the effective thermal conductivity. This can be attributed to the decrease in the temperature drop between the extreme ends of the heat pipe, as seen earlier in Fig. 14. An increase in the condenser length affects the effective thermal conductivity in a way similar to an increase in the condenser heat transfer coefficient. The effect of an increase in the condenser length on the effective thermal conductivity is shown in Fig. 21.

Comparison with Microheat Pipe of Triangular Cross Section

A comparison is presented in Table 6 between the calculated values of the effective thermal conductivity of the wire-sandwiched microheat pipe without an adiabatic section, and a triangular microheat pipe array [14] having equilateral triangular channels, the geometry of which has been mentioned earlier in the previous section, for identical length and input heat flux values. The values corresponding to the triangular microheat pipe [14] have been recalculated for a cross-sectional area equal to that of the wire-sandwiched microheat pipe under consideration, and presented in the table. It is to be noted that the values of the effective thermal conductivity obtained are larger for the wire-sandwiched microheat pipe, for the particular geometric configuration. Though this observation cannot be generalized for all geometric dimensions, it is obvious that the two designs offer comparable performances. Along with this, the ease of fabrication of the wire-sandwiched microheat pipe also holds the potential to make the use of this device an attractive option in thermal management of microelectronics.

Conclusions

A detailed mathematical model for fluid flow and heat transfer in a wire-sandwiched microheat pipe channel is presented in this paper, which is used in determining the field variables inside the channels and evaluating the performance of the device. The distribution of the velocity, temperature, and pressure were obtained, and the performance evaluated by calculating the effective thermal conductivity resulting from various conditions of input heat flux values and

geometric parameters. A comparison is made between the performance of the wire-sandwiched microheat pipe and that of a triangular heat pipe of the same cross-sectional area for identical operating conditions.

Based on the analysis, the following conclusions are made for the wire-sandwiched microheat pipe:

1) The minimum meniscus radius for the liquid–vapor interface occurs at the beginning of the evaporator section, and the maximum occurs at the end of the condenser section.

2) The steady-state effective thermal conductivity increases with heat input due to the reduction in the temperature drop along the microheat pipe. Because of a higher temperature drop, the effective thermal conductivity decreases with an increase in the condenser heat transfer coefficient, the wire diameter, and the pitch of the wires.

From a comparison at identical input heat flux values, it is noticed that the wire-sandwiched microheat pipe can offer a performance comparable to that of the triangular microheat pipe of identical cross-sectional area. Also, the ease of fabrication makes the wire-sandwiched heat pipe design an attractive option for applications such as thermal management of miniature electronic systems and devices.

References

[1] Garimella, S. V., and Sobhan, C. B., "Recent Advances in the Modeling and Applications of Nonconventional Heat Pipes," *Advances in Heat Transfer*, Vol. 35, 2001, pp. 249–308.

[2] Cotter, T. P., "Principles and Prospects of Microheat Pipes," *Proceedings of the 5th International Heat Pipe Conference*, Tsukuba, Japan, 1984, pp. 328–335.

[3] Peterson, G. P., and Sobhan, C. B., "Applications of Microscale Phase Change Heat Transfer: Micro Heat Pipes and Micro Heat Spreaders," *The MEMS Handbook*, 2nd ed., Vol. 3, Applications, CRC Press, Boca Raton, FL, 2005.

[4] Wang, Y. X., and Peterson, G. P, "Analysis of Wire-Bonded Micro Heat Pipe Arrays," *Journal of Thermophysics and Heat Transfer*, Vol. 16, No. 3, 2002, pp. 346–355.

[5] Babin, B. R., Peterson, G. P., and Wu, D., "Steady-State Modeling and Testing of a Micro Heat Pipe," *Journal of Heat Transfer*, Vol. 112, 1990, pp. 595–601.

[6] Chi, S. W., *Heat Pipe Theory and Practice*, McGraw–Hill, New York, 1976.

[7] Khrustalev, D., and Faghri, A., "Thermal Analysis of a Micro Heat Pipe," *Journal of Heat Transfer*, Vol. 116, 1994, pp. 189–198.

[8] Wu, D., and Peterson, G. P., "Investigation of the Transient Characteristics of a Micro Heat Pipe," *Journal of Thermophysics and Heat Transfer*, Vol. 5, April–June, 1991, pp. 129–134.

[9] Wu, D., Peterson, G. P., and Chang, W. S., "Transient Experimental Investigation of Micro Heat Pipes," *Journal of Thermophysics and Heat Transfer*, Vol. 5, No. 4, 1991, pp. 539–545.

[10] Longtin, J. P., Badran, B., and Gerner, F. M., "A One-Dimensional Model of a Micro Heat Pipe During Steady-State Operation," *Journal of Heat Transfer*, Vol. 116, 1994, pp. 709–715.

[11] Peterson, G. P., and Ma, H. B., "Temperature Response and Heat Transfer in a Micro Heat Pipe," *Journal of Heat Transfer*, Vol. 121, No. 2, 1999, pp. 438–445.

[12] Hopkins, R., Faghri, A., and Khrustalev, D., "Flat Miniature Heat Pipes with Micro Capillary Grooves," *Journal of Heat Transfer*, Vol. 121, No. 1, 1999, pp. 102–109.

[13] Ma, H. B., Peterson, G. P., and Peng, X. F., "Experimental Investigation of Counter-Current Liquid-Vapor Interactions and its Effect on the Friction Factor," *Experimental Thermal and Fluid Science*, Vol. 12, No. 1, 1996, pp. 25–32.
doi:10.1016/0894-1777(95)00064-X

[14] Sobhan, C. B., Xiaoyang, H., and Yu, L. C., Investigations on Transient and Steady-State Performance of Micro Heat Pipe," *Journal of Thermophysics and Heat Transfer*, Vol. 14, 2000, pp. 161–169.

[15] Sobhan, C. B., and Peterson, G. P., "Modeling of the Flow and Heat Transfer in Micro Heat Pipes," *Second International Conference on Microchannels and Minichannels*, American Society of Mechanical Engineers, Rochester, NY, 2004.

[16] Sobhan, C. B., Rag, R. L., and Peterson, G. P., "A Review and Comparative Study of the Investigations on Micro Heat Pipes," *International Journal of Energy Research*, Vol. 31, Nos. 6-7, 2007, pp. 664–688.
doi:10.1002/er.1285

[17] Launay, S., Sartre, V., and Lallemand, M., "Investigation of a Wire Plate Micro Heat Pipe Array," *International Journal of Thermal Sciences*, Vol. 43 5, 2004, pp. 499–507.
doi:10.1016/S1290-0729(00)00205-2

[18] Faghri, A., *Heat Pipe Science and Technology*, Taylor & Francis Group, 2 Park Square, Abingdon 1995, Chap 10.

[19] Bejan, A., *Convection Heat Transfer*, 3rd ed., Wiley, Hoboken, NJ, 2004.

[20] Peterson, G. P., *An Introduction to Heat Pipes*, Wiley, New York, 1994.

[21] Vadakkan, U., Garimella, S. V., and Sobhan, C. B., "Characterization of Performance of Flat Heat Pipes for Electronics Cooling," The Electrical and Electronic Pacjaging Division (EEP), Vol. 28, Packaging of Electronic and Photonic Devices, American Society of Mechanical Engineers, Fairfield, NJ, 2000.

[22] Sobhan, C. B., and Peterson, G. P., *Microscale and Nanoscale Heat Transfer:Fundamentals and Engineering Applications*, Taylor and Francis/CRC Press, Boca Raton, FL, 2008.